Check for updates

Received: 5 July 2023 | Revised: 22 September 2023 | Accepted: 3 October 2023

DOI: 10.1002/eng2.12799

RESEARCH ARTICLE

Engineering Reports Open Access WILEY

Numerical multiscale analysis of 3D printed short fiber composites parts: Filament anisotropy and toolpath effects

Alejandro Estefani | **Luis Távara**

Grupo de Elasticidad y Resistencia de Materiales, Escuela Técnica Superior de Ingeniería, Universidad de Sevilla, Sevilla, Spain

Correspondence
Luis Távara, Grupo de Elasticidad y Resistencia de Materiales, Escuela Técnica Superior de Ingeniería, Universidad de Sevilla, Camino de los Descubrimientos s/n, 41092 Sevilla, Spain.
Email: ltavara@us.es

Funding information
Ministerio de Economía y Competitividad, Grant/Award Number: PID2021-123325OB-I00

Abstract

The aim of the present investigation is the development of a numerical model able to adequately represent the effect of several variables, associated to the fused deposition modeling (FDM) procedure, on the mechanical behavior of 3D printed parts. Specifically, 3D printed carbon short-fiber reinforced thermoplastic parts are numerically analyzed. Previous experimental results have proven that this kind of parts show a global anisotropic behavior, in terms of classical mechanical parameters as stiffness. Thus, special emphasis is done in analyzing the effect of the raster angle / toolpath (inherent to FDM) and the internal microstructure of the deposited filaments (due to the presence of the short fibers). Multiscale finite element models are used to represent the linear elastic behavior at macro scale. The numerical models are also able to include the effect of porosity. Based on experimental results of 3D printed composite parts with 100% infill and different raster angles, elastic transversely isotropic properties are estimated for the individual deposited filaments using a reverse engineering procedure. Obtained results show that for an adequate modeling of FDM composite parts, anisotropic properties of the filament must be taken into account, even when quasi-isotropic printing parameters are used ("cross-ply" configurations). Finally, additional numerical analyses of some parameters associated to the FDM technique are done. Specifically, the effect of porosity related to the infill pattern and percentage on the global (macro) apparent stiffness is analyzed.

KEYWORDS

3D printing, ALM, filament anisotropy, multiscale FEM, toolpath effect

1 | INTRODUCTION

Additive manufacturing (AM) processes have attracted the interest of the scientific and industrial community for their ability to generate parts with complex geometries without adding extra cost. In conventional manufacturing processes, there is a direct relationship between the cost of a component and the complexity of its geometry, and this relationship is not established directly by AM processes. In particular, AM manufacturing processes are of interest to composite material manufacturers. This is due to this technology is capable of creating parts with a higher degree of complexity (inclusion of

This is an open access article under the terms of the Creative Commons Attribution License, which permits use, distribution and reproduction in any medium, provided the original work is properly cited.
© 2023 The Authors. *Engineering Reports* published by John Wiley & Sons Ltd.

ribs, recesses, areas of different curvature, etc.), but it is also possible to reduce manufacturing cycle times and inherent costs. Among the different AM methods, selective laser sintering (SLS) and additive layer manufacturing (ALM) are the most suitable due to lower energy and material costs, as well as greater design accuracy and minimum waste materials. Moreover, the new tendencies in industry includes the use of ALM 3D printing technique not only for prototyping but also for the manufacturing of structural parts with loading capacity. Thus, it is a key issue to have an accurate understanding of the mechanical behavior of ALM parts. Some of their appealing characteristics are related to sostenibility that should be taken into account at every design and manufacturing steps. In this sense, the use of thermoplastics (commonly used in ALM procedures) allow several recycling strategies. On the other hand, the improvement of the mechanical properties of this kind of plastics can be achieved by the inclusion of reinforcements as short or continuous fibres, that is, obtaining a composite material.

In the recent years composites development have grown considerably. Nowadays, its use in light-weight structures includes safety, behavior and realibility requirements. Nevertheless, there are still several aspects to be analyzed for a wider use of composites. Some of these aspects are related to the manufacturing process sostenibility and reciclability. That is why, the use of thermoplastic based composites are gaining importance lately.[1] The use of thermoset based composites and established manufacturing processes are nowadays associated with high production times and related cost increments. Moreover, this processes generate a large amount of scrap material producing a costly life cycle.

An alternative to classical manufacturing processes is ALM. In particular fused deposition modeling (FDM) allows the use of raw materials that can be reused, for example, thermoplastics. An interesting example is shown in Reference 2, where a novel FDM technique that includes recycling and remanufacturing of PLA reinforced with continuous carbon fibres is presented. It is remarkable that tensile and bending strength performance was better for remanufactured parts. With regard to the effects on dimensional stability of thermoplastics parts, the mechanical properties and thermal properties, carbon and glass fibre reinforcements are of interest, but also reinforcements of natural origin. In Reference 3, the behavior of filaments made of an ABS matrix reinforced with oil palm is presented. Specifically, strength, stiffness, dimensional stability and void ratio of materials manufactured by FDM are analyzed, concluding the improvement in average stiffness and strength as the weight proportion of oil palm increases. In Reference 4, the rheological properties of the inclusion of HBN fillers in ABS is studied, with positive effects in terms of viscosity and no differences with respect to ABS pellets except by their thermal conductivity behavior. A review on the use of this 3D printing technology including relevant aspects associated with materials, CAD models, prototyping, freedom on customized design and deposition techniques can be found in References 5,6. Nowadays, 3D printing is being used in different kinds of industries and applications. Some examples includes its use in biomedical applications, for example, bone and organ regeneration,[7] hip protheses,[8] and personalized sockets for amputed zones.[9] In the aeronautics field, the manufacturing of rotors[10] or even the entire fuselage[11] of unmanned aircraft vehicles (UAV) are good examples of the current 3D printing usage. Although there is a great variety of polymers that can be used in FDM, obtained mechanical properties are usually worse (in terms of stiffness and strength) than those obtained with other high-tech materials as metals or composites. Moreover, parts manufactured by FDM usually generates holes and pores, associated with the filament deposition, limiting its applicability. Thus, several authors have analyzed the properties obtained by reinforcing those thermoplastic polymers with continuous fibres. Behavior under tensile loading is analyzed in References 12,13. The effect of temperature and pressure in the adhesion of layers as well as in the carbon fibre content is analyzed in Reference 14. It is interesting to notice that the inclusion of carbon fibres in 3D printed parts improved the mechanical properties of the polymeric matrix. New developments in 3D printing techniques allowed to have panels with variable stiffness allowing a better buckling performance. A numerical analysis of this kind of configurations including critical buckling load and non-linear failure mode analyses is presented in Reference 15. In Reference 16, inter and intra laminar fracture properties of polyamide reinforced with continuous carbon fibre is studied. The above mentioned investigations, among others, have proven that the use of continuous fibres is the best option to improve the mechanical properties of a thermoplastic matrix. Nevertheless, in parts with complex geometries (as those designed for 3D printing) is not always feasible to include a continuous fibre reinforcement everywhere. In particular, these zones are related to abrupt changes in the geometry which also coincides with stress raiser zones (i.e., corners, notches, etc.).[17] An intermediate solution is the use of polymers reinforced with short fibres in those critical zones. The resulting composite including short fibres present better properties than those obtained using the polymeric matrix without reinforcement.[18] Other investigations have also analyzed the tensile, bending and impact behavior of these kind of 3D printed composites.[19,20] The printing bed position and the infill percentage effect on the dimensional control and obtained mechanical properties of 3D printed coupons is shown in Reference 21. More recently, experimental results of tensile and fracture toughness tests of coupons made of Onyx® (a commercial filament including short carbon

25778196, 0, Downloaded from https://onlinelibrary.wiley.com/doi/10.1002/eng2.12799 by Universidad De Sevilla, Wiley Online Library on [08/11/2023]. See the Terms and Conditions (https://onlinelibrary.wiley.com/terms-and-conditions) on Wiley Online Library for rules of use; OA articles are governed by the applicable Creative Commons License

fibres embedded in a nylon matrix supplied by Markforged®[22]) showed a clear anisotropic behavior.[23] Similar conclusions were obtained for ABS coupons manufactured by FDM under tensile, bending and impact loading.[24,25]

Regarding the research focused in the numerical simulation of this kind of materials. In Reference 26, the damage onset and growth of CT coupons is analysed using the Phase Field fracture model. Other studies used the extended finite element model (XFEM) including a Cohesive Zone Model (CZM) to analyse the fracture properties and failure modes of Single Edge Notched Bending (SENB) of ABS specimens manufactured by FDM.[27,28] Nevertheless, the numerical models found in literature do not take into account the anisotropy inherent to the FDM technique and the filament microstructure. One option, to overcome this issue, is the use of a multiscale modeling framework. In this sense, the Representative Volume Element (RVE) concept should be used at a micro scale based on the orientation averaging to predict the macroscopic behavior.[29] Several homogenization procedures could be used to get the equivalent properties of the RVE.

Consequently, the aim of the present research is to present an accurate and systematic multiscale finite element model for parts manufactured by FDM. First, the equivalent elastic transversely isotropic properties of a single printed filament are obtained. The estimation of the properties is obtained by means of a reverse engineering procedure and data from experimental testing. The developed numerical model links different scales from deposited filament level to homogeneous (macro) coupon level. This model is able to include the raster angle, infill pattern and porosity inherent to the FDM procedure. Once the model is calibrated, the effect of the listed parameters over the overall stiffness of the specimens is studied. It is interesting to recall that the feasibility to have an accurate tool allows the generation of digital twins. These models could help designers and engineers in the optimization of parts and structures manufactured by FDM.

2 | FDM COUPLED NUMERICAL MODEL

In this section, first some basic aspects of the FDM procedure that an accurate modeling should include are briefly described. Then, the developed numerical simulation scheme is detailed.

In FDM, the printer is feed by thermoplastic based filaments (that may be reinforced or not). The filament goes through a heated noozle, then the fused filament is deposited in rows. When 100% infill is chosen, the filaments are put side by side, forming a layer. Once a layer is done, a new layer is printed over the previous one finally obtaining a solid part. The noozle translate along the plane parallel to the printing bed following location orders (toolpath) introduced by a file.

In the present research, the properties associated to Onyx® filaments and printing parameters of MarkTwo® printer will be used. Nevertheless, it should be noted that the proposed procedure could be applied to any other filament reinforced with short fibres.

Onyx is formed by a nylon matrix reinforced with chopped carbon fibres, thus becoming a composite material. The fibres represent the 12.8% in weight and most of them are aligned following the axial direction of the filament. The filament diameter prior printing is 1.75 mm. The short fibres are prisms with a variable section with non regular area that may be represented by an ellipse, being the mean major axis around 7.4 μm. Recalling the fibres length there is great variability, being the shortest and the largest measured fibres around 6.4 and 246 μm, respectively, see Reference 23 for additional details of the measurements.

Recalling printing parameters, some of the most relevant ones are described in the following: (a) nozzle temperature: 265°C, (b) thickness of each printed layer: 0.125 mm, (c) dimensional accuracy (xy) $\pm$ 250 μm, (d) dimensional accuracy (z) $\pm$ 100 μm, and (e) Maximum build volume (W $\times$ D $\times$ H): $320 \times 132 \times 154\,\text{mm}^3$. It should be noted that these printing parameters are fixed in the MarkTwo® printer.

2.1 | General aspects of the numerical model

The developed numerical model is a combination of mechanical simulations of several configurations of the tensile test that includes the effect of the FDM parameters at different scales. A summary of the experimental procedure that will be modeled is shown in Figure 1.

One of the key parameters in FDM is the toolpath, which is the trajectory followed by the noozle when the filaments are deposited in a layer. The sum of the layers results in the final printed part. Each layer can have a different toolpath. The toolpath can be represented as set of polylines placed on a horizontal plane parallel to the printing bed. Figure 2 shows an scheme of the coupled numerical model. It includes the equivalent properties of the fused filament, the toolpath and porosity due to the gaps between the filaments.

25778196, 0, Downloaded from https://onlinelibrary.wiley.com/doi/10.1002/eng2.12799 by Universidad De Sevilla, Wiley Online Library on [08/11/2023]. See the Terms and Conditions (https://onlinelibrary.wiley.com/terms-and-conditions) on Wiley Online Library for rules of use; OA articles are governed by the applicable Creative Commons License

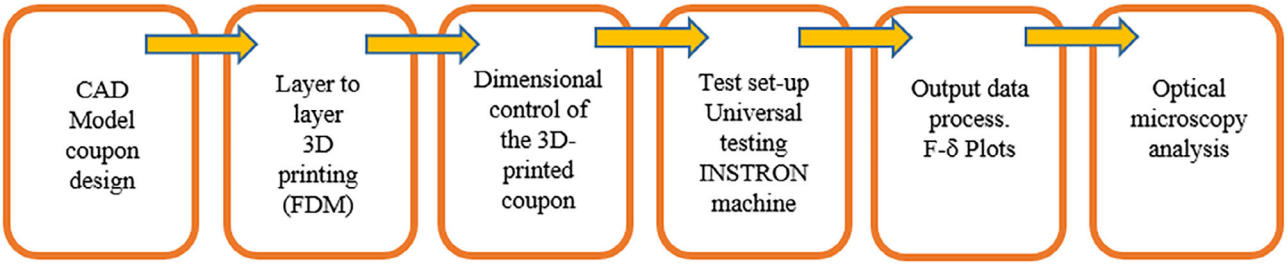

FIGURE 1 Flowchart of the experimental procedure.

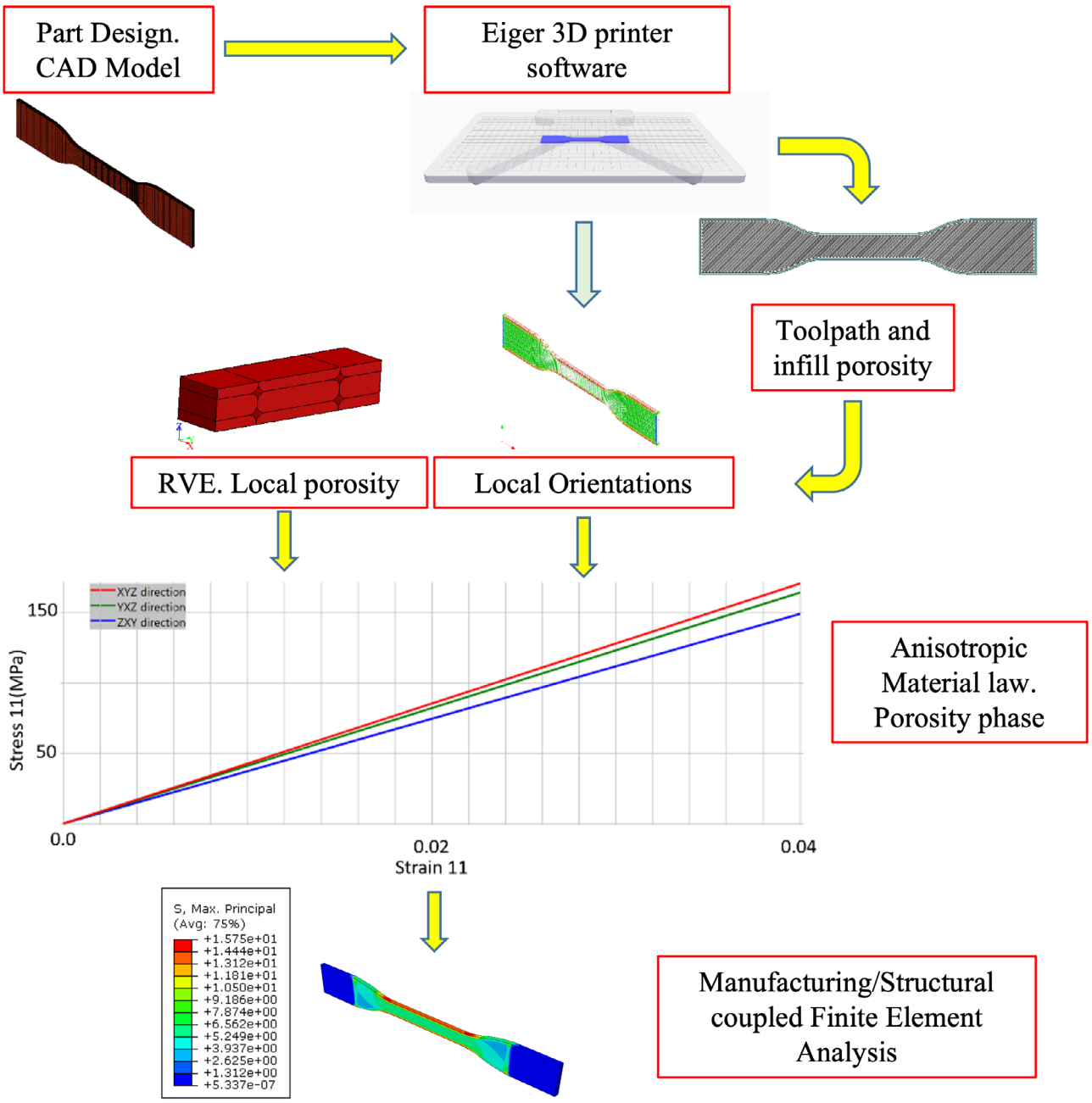

FIGURE 2 Customised workflow of FDM coupled numerical model.

25778196, 0, Downloaded from https://onlinelibrary.wiley.com/doi/10.1002/eng2.12799 by Universidad De Sevilla, Wiley Online Library on [08/11/2023]. See the Terms and Conditions (https://onlinelibrary.wiley.com/terms-and-conditions) on Wiley Online Library for rules of use; OA articles are governed by the applicable Creative Commons License

First, a CAD model of the part to be printed is needed. Next, a slicer software is needed for the identification of the printing parameters. Eiger® slicer software is used for the MarkTwo®printer. The file generated by Eiger® is then imported in the multiscale modeling software Digimat®.[30] It allows to get the toolpath generated by Eiger and also to export this information (in terms of a local orientation tensor at integration point level) to several FEM softwares. Moroever, based on the RVE concept, Digimat is also able to include the effect of porosity induced by the gaps between deposited filaments. Finally, the mechanical model including desired boundary conditions is done, in the present research the FEM software Abaqus®[31] is used.

The analysed model simulates a tensile test. The geometry and dimensions of the specimens are based on ASTMD 638-14 standard,[32] see Figure 3. It is interesting to notice that the FDM toolpath includes a lateral wall at every layer which follows the external boundary of the specimen. The wall is formed by a single deposited filament of 0.4 mm width. Once the wall is done the inner part (infill) of the specimen is printed following the desired pattern.

2.2 | Multiscale approach

Due to the filament deposition follows different trajectories and angles (toolpath) one or several preferent directions could appear in the final part. In Figure 4, two different toolpaths are shown. Moreover, the presence of short fibres within the filament that are mainly aligned with the printing direction produces an equivalent anisotropic behavior of the part. As a consequence the overall stiffness is affected by these parameters.

Recalling, the anisotropy behavior of the filament, it could be simplified to a transversely isotropic behavior (as done in classical CFRPs).[33] Besides, the presence of large pores is also associated with FDM (due to the gaps between deposited filaments), being an important parameter in the equivalent material model. It should noticed that the geometry of these pores may also affect the overall anisotropy of the part.

In Figure 5, the multiscale approach (based on the RVE concept) is depicted. The numerical treatment for the multiscale transition is summarized in the following:

1. At macro mechanical level: Each integration point of the 3D structural FEM model is typically associated to the RVE center. At this scale, the material behavior is assigned to the geometry to be modeled. Equivalent homogeneous properties are assigned to each element according to the RVE corresponding to that location.

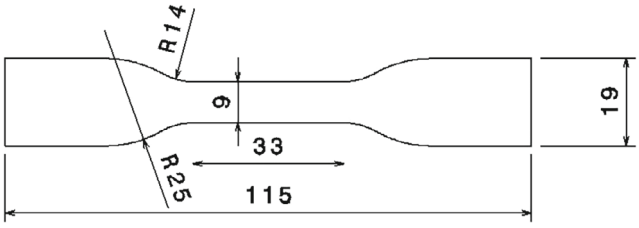

FIGURE 3 Specimen dimensions thickness $T = 2$ mm.

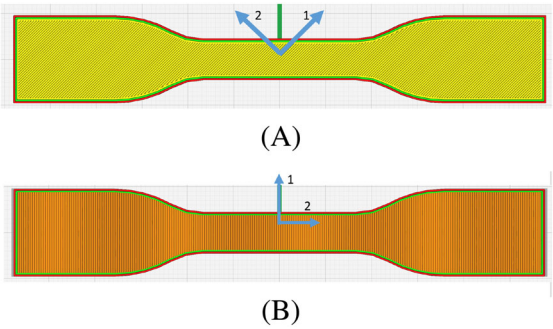

FIGURE 4 Toolpath orientation at a layer with (A) 45°, and (B) 90°.

25778196, 0, Downloaded from https://onlinelibrary.wiley.com/doi/10.1002/eng2.12799 by Universidad De Sevilla, Wiley Online Library on [08/11/2023]. See the Terms and Conditions (https://onlinelibrary.wiley.com/terms-and-conditions) on Wiley Online Library for rules of use; OA articles are governed by the applicable Creative Commons License

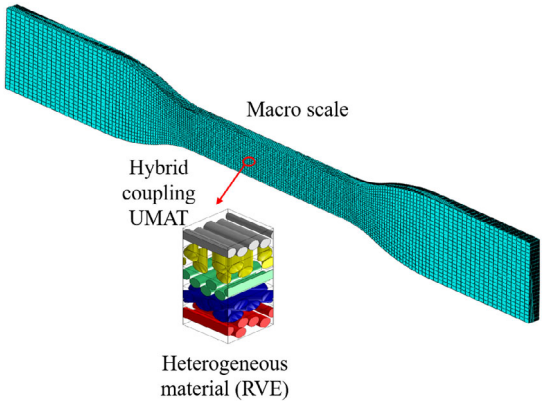

FIGURE 5 Coupled analysis using implicit FEA solver.

2. At meso scale: The RVE consist of a certain number of constituents. From a computational point of view including the constituents behavior directly to a macro scale model will result in a large amount of elements. Moreover, this model may not be solved if the number of elements is too large. In the present investigation, the RVE is made up of the different fused filaments and their stacking sequence, obtaining a lattice kind structure. Thus, it is also possible to include the holes (pores) that may appear between adjacent deposited filaments. Probability functions related to orientations and different boundary conditions can be applied to the RVE. As a result, constitutive laws are obtained at macro level.
3. Material constitutive model for each printed filament: According to Onyx datasheet, an isotropic behavior is assumed being its Young's Modulus value between 1.4 and 2.4 GPa. Nevertheless, experimental testing of quasi-isotropic printed specimens with +45/−45 and 0/90 stacking sequence configurations showed differences on the overall mechanical behavior. These results indicate that the filaments can not have an isotropic behavior. The anisotropy is induced by the presence of aligned fibres due to the nature of the manufacturing process. Then, a feasible assumption could be the use of transversely isotropic properties. Thus, a uniform behavior along a plane is expected (i.e., perpendicular to z-direction) while a different behavior occur at the perpendicular direction. In this sense, five parameters are needed to define the filament behavior.[34]
4. Transition algorithm: By means of a homogenisation algorithm, included in Digimat, a macroscopic constitutive law is obtained for the RVE. Thus the mean stress and strain values are obtained for each phase of the RVE.[29]
5. The communication between scales is done by means of Abaqus® dynamic UMAT subroutines created by Digimat®. They include the equivalent properties of the RVE and translate this information to the integration points of the macro scale FEM model. UMAT calculates the tangent stiffness matrix and updates it at every iteration.

2.3 | Details of the manufacturing/mechanical coupled models

From an operational point of view, the 3D printing design and manufacturing process are summarized in the following steps:

1. A CAD tool is used to design the specimen. Then the geometry is exported in a STL format. This format describes the geometry surface as a set of triangles. This format is usually used in 3D printers.
2. The STL file is imported in the slicer software of the printer. Markforged printers uses an online software called Eiger®.
3. Eiger® allows to locate the specimen within the printing bed, to select the printing material (filaments) and to determine some printing parameters. The different available filaments include Onyx and nylon reinforced with continuous fibres (carbon, glass and kevlar). Regarding the printing parameters, Eiger allows to choose the infill pattern, the way the reinforcement is used, use of brim, and so forth. The software divides the process layer by layer and determines the printing path for each individual layer.

25778196, 0, Downloaded from https://onlinelibrary.wiley.com/doi/10.1002/eng2.12799 by Universidad De Sevilla, Wiley Online Library on [08/11/2023]. See the Terms and Conditions (https://onlinelibrary.wiley.com/terms-and-conditions) on Wiley Online Library for rules of use; OA articles are governed by the applicable Creative Commons License

4. Eiger translate all the printing information to a MFP file. This file is transferred to the printer via online or a USB drive. Then, the specimen is printed layer by layer. The chosen parameters and materials control the final geometrical dimensions, surface finishing, printing time and mechanical properties of the printed part.

In order to adequately couple the FDM process to the structural analysis, the 3D printing trajectory should be mapped in the FEM structural model. For this purpose, the 3D printing trajectory information is transferred, in terms of a "local orientation tensor" that describes the raster angle, to each integration point of the 3D finite element mesh. This local orientation tensor is described by the symmetric (3×3) matrix a_{ij}, which defines an orientation distribution on the volume element. The orientation tensor is a measure of the probability of finding filaments in a given area of the "RVE" oriented with a preferred direction. The set of orientation tensors for each integration point forms the trajectory map followed by the printer.

A 3D mapping algorithm based on a integration point-node approach is used. A "donor mesh" including orientation tensor, residual stress and/or temperature data transfer the information to a "recipient mesh" where the data of interest is mapped. This procedure includes the following steps:

1. Identify the integration points of the "recipient mesh", that is, the structural model mesh.
2. Locate these integration points on the "donor mesh" space and select the associated triangular elements (STL file).
3. Sample the filaments associated to the trajectory map in the "donor mesh" that are located close to the identified integration points and obtain the average orientation tensor.
4. Finally, the orientation tensors are transferred to the "recipient mesh". The results are obtained by either an interpolation or extrapolation of the integration point data to the mesh nodes, thus averaging or smoothing the results.

In the mapping procedure between both meshes, there is not always a perfect correspondence between elements to be mapped and integration points where the results are evaluated. As a consequence, there will be nodal results of the "recipient (structural) mesh" that have to be averaged based on a computational tolerance that depends on the size of the elements of the donor mesh.

Figure 6 shows a graphical representation of the described procedure for the tensile test on specimens oriented at +45/−45. On the one hand, the data associated with the manufacturing process (geometry and deposition path of the filaments) is described. On the other hand, the data associated with the structural problem of the tensile test, including

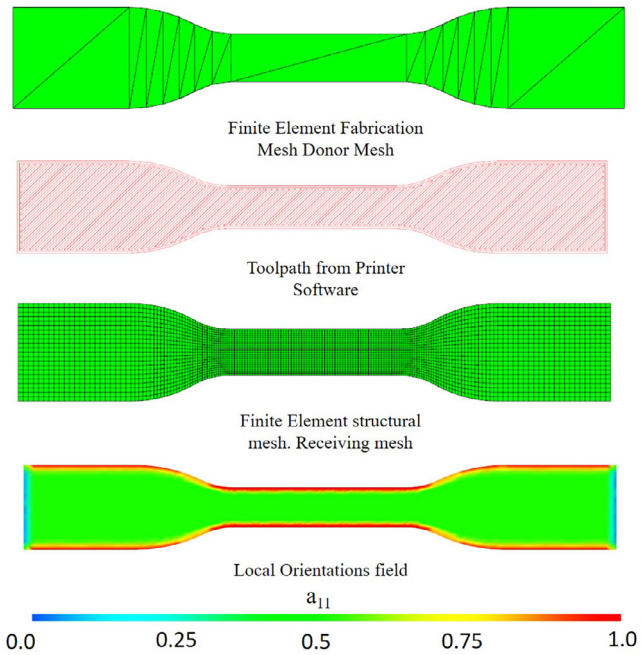

FIGURE 6 Mapping approach combining FDM toolpath and structural FEM. a_{11} is dimensionless value of the local orientation tensor, in the analysed models 0 and 1 represent the vertical and horizontal directions, respectively.

25778196, 0, Downloaded from https://onlinelibrary.wiley.com/doi/10.1002/eng2.12799 by Universidad De Sevilla, Wiley Online Library on [08/11/2023]. See the Terms and Conditions (https://onlinelibrary.wiley.com/terms-and-conditions) on Wiley Online Library for rules of use; OA articles are governed by the applicable Creative Commons License

loads and boundary conditions, are imposed. Using both models, the data transfer is able to generate the orientation and/or porosity tensor map of the RVE to be included in the coupled model.

Once the FDM problem is connected to the structural analysis through the "mapping" of the toolpath. The porosity phase at the meso-scale could also be included. This porosity is associated to certain printing patterns depending on the infill percentage and pattern (shape of the lattice). Operationally, this porosity is associated with the filament deposition as discussed in the previous section and which depends mainly on the width of the printed filaments, in this case 0.4 mm. In the first analysis included in the present research, no porosity phase is included as the characterisation of Onyx is aimed and infill 100% is used. Then, some lattice patterns are analyzed and associated porosity phases are used.

The bridging between the different modeling levels is done by weak coupling. In this sense, to evaluate the macroscopic mechanical response (in terms of forces, stresses, strains or damage parameters) homogenisation techniques of the RVE are used to calculate the stiffness tangent matrix. For this purpose, a large number of simulations with the chosen constitutive law and parameterisation of the "RVE" (for a given number of preferred orientations and applied loads) is done. This step allows generating a database of the material under different loading configurations. It is a previous step to solve using the implicit solver of ABAQUS. From a practical point of view, it could be considered equivalent to launching a large campaign of experimental tests including various orientations and loads. For each orientation, the meso-scale model is identified. The set of "meso" models defines the final model at the macro scale. A dynamic user material subroutine (UMAT) is created by Digimat® for each integration point of every structural 3D element. The original orientation tensor of the toolpath is interpolated or extrapolated to locally rotate the material coordinate system and couple the 3D printing trajectory as input data. Depending on each orientation, the stiffness properties associated with the material database of the meso model, previously calculated, are evaluated at each integration point.

3 | LINEAR ELASTIC ONYX CHARACTERIZATION: REVERSE ENGINEERING

The aim of this section is to determine the equivalent properties of each deposited Onyx filament. It should be recalled that MarkForged printing parameters do not allow to manufacture unidirectional specimens. As the 100% infill pattern tends to generate quasi-isotropic macroscopic properties by printing the layers following a cross-ply sequence (i.e., +45/−45 or 0/90). Nevertheless, experimental results showed that 0/90 and +45/−45 specimens present a very different behavior. This results clearly indicate that each deposited onyx filament present an anisotropic behavior. The reverse engineering procedure is based on the numerical solution of several FEM models including different anisotropic properties for the deposited filaments and infill patterns that are compared with the corresponding experimental data. The variable that is chosen for comparison is the apparent stiffness in the loading direction obtained in the FEM models and the experiments.

From a microscopical point of view, the fused filaments includes fibres oriented in a preferential direction. Thus, a homogenized transversely isotropic behavior can be considered at mesoscale.[34] Then, five variables are needed to characterise this behavior: E_{11}, E_{22}, G_{12}, G_{23}, ν_{12}. Being 1 associated to the printing direction, while 2 and 3 are the direction of the fused filament cross section.

Based on anisotropic elasticity, G_{23} can be related to E_{22} and ν_{23} by:

$$G_{23} = \frac{E_{22}}{2(1+\nu_{23})} \tag{1}$$

It should be recalled that ν_{23} and G_{23} values are not easily obtained from experiments. Thus, in the present study the following assumptions are taken:

1. ν_{23} and ν_{12} are set from the bibliography.[34]
2. G_{12} is set equal to G_{23} and they are determined using (1).
3. E_{11} and E_{22} becomes the only independent parameters to be determined by the reverse engineering procedure.

Table 1 summarizes the input data that generate the (5×6) matrix of FEM models to be solved which is the base of the reverse engineering procedure to determine the equivalent properties of each deposited Onyx filament. The obtained apparent stiffness is then compared to both test configurations: 45/−45 and 0/90. The stiffness E_{11} is increased in increments of 2400 MPa, while E_{22} is increased in increments of 240 MPa. The rest of the variables are obtained as indicated in the previous paragraph.

25778196, 0, Downloaded from https://onlinelibrary.wiley.com/doi/10.1002/eng2.12799 by Universidad De Sevilla, Wiley Online Library on [08/11/2023]. See the Terms and Conditions (https://onlinelibrary.wiley.com/terms-and-conditions) on Wiley Online Library for rules of use; OA articles are governed by the applicable Creative Commons License

TABLE 1 Properties used in the reverse engineering procedure.

Property	E_{11} (MPa)	E_{22} (MPa)	ν_{12}	ν_{23}	$G_{12} = G_{13}$ (MPa) (1)
Min	2400	480	0.32	0.45	165
Max	7200	2880	0.32	0.45	993
Increments	1200	480	—	—	165

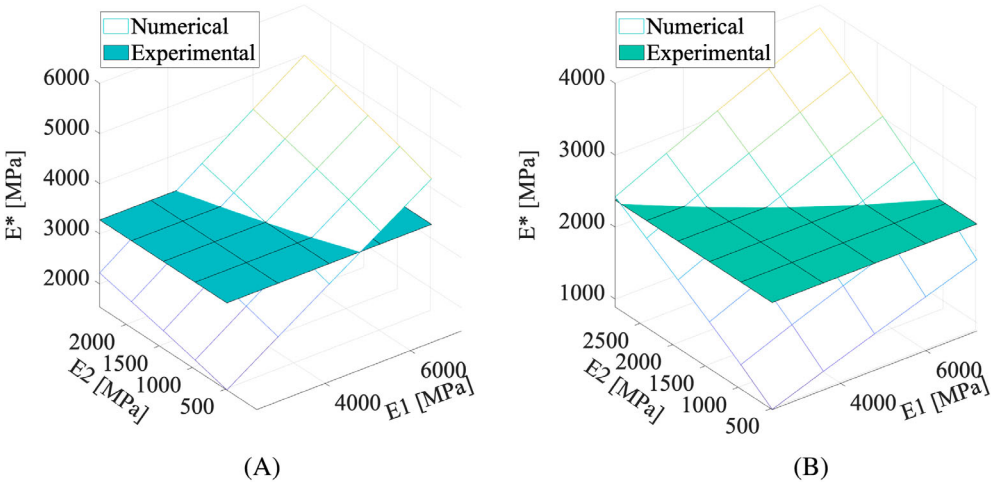

FIGURE 7 Obtained numerical apparent stiffness (E*) and mean experimental apparent stiffness for: (A) +45/−45 configuration and (B) 0/90 configuration.

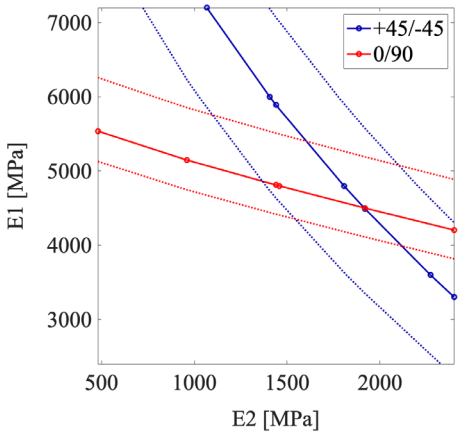

FIGURE 8 Isolines corresponding with the intersection of the obtained numerical models and the experimental data.

From the coupled numerical model, the resultant force on a tensile test configuration under displacement control is obtained. With this FEM value, the numerical stress-strain virtual behavior curve is evaluated for a tensile test specimen (Figure 3) in the centre zone along 25 mm. This length was chosen to be equal to the zone where the extensometer was located in the experimental campaign.

The different pairs (E_{11} and E_{22} values) produces a surface that describes the obtained apparent stiffness, see Figure 7. The intersection of this surface with the plane associated with the obtained experimental apparent stiffness creates an isoline that represent the values that adequately models the mechanical behavior. The intersections for 0/90 and +45/−45 configurations using the mean experimental values are presented in Figure 7A,B, respectively. In Figure 8, the continuous lines represent the isolines obtained using the mean experimental value of the apparent stiffness. The discontinuous lines

25778196, 0, Downloaded from https://onlinelibrary.wiley.com/doi/10.1002/eng2.12799 by Universidad De Sevilla, Wiley Online Library on [08/11/2023]. See the Terms and Conditions (https://onlinelibrary.wiley.com/terms-and-conditions) on Wiley Online Library for rules of use; OA articles are governed by the applicable Creative Commons License

represent the isolines obtained using the minimum and maximum experimental values of the apparent stiffness. Blue lines are associated with +45/−45 configuration while red lines are associated to 0/90 configuration. Thus, the zone where the isolines converges represent E_{11} and E_{22} values that correctly represent the behavior on both test configurations.

Table 2 shows the optimised properties determined by the reverse engineering procedure to numerically characterize the transversely isotropic behavior of the fused filament.

4 | NUMERICAL-EXPERIMENTAL CORRELATION

The aim of this section is to evaluate the accuracy and reliability of the numerical model. On the one hand, the apparent stiffness is analysed as a function of the toolpath of the deposition process for specimens with 100% infill and two quasi-isotropic configurations 0/90 and +45/−45. On the other hand, the porosity effects associated with the FDM process itself and different infill patterns is studied. Further details associated with the testing campaign and the cases tested can be found in Reference 23.

4.1 | Manufacturing of 100% infill FDM specimens

As mentioned previously, the specimens are manufactured with the MarkTwo printer from the company Markforged. The dimensions of the specimens are shown in Figure 3. There is no specific standard for testing 3D printed short fibre reinforced thermoplastics, so ASTM D638 is used as a basis. It should be noted that the width used in the centre cross-section is larger than the limits set by the standard. This decision was taken in order to have bigger area of material with preferred orientations. The design of the specimens is done using a CAD software, generating the STL files. Then, it is imported to Eiger slicer software. Then, the part is printed by depositing layers of Onyx filaments. After deposition, the filaments cool down and as result a solid part with adequate dimensional stability and stiffness is obtained. Figure 9 shows a micrograph of a 0/90 specimen cross-section at 10× magnification showing the distribution of the short fibre reinforcements that characterize the material under study. This micrograph allows us to identify the short fibres with the preferred orientations according to the test trajectory. Moreover, large porosity zones can be clearly seen. Similar observations were reported in Reference 23.

TABLE 2 Fitted properties determined by the reversed engineering procedure.

E_{11} (MPa)	E_{22} (MPa)	ν_{12}	ν_{23}	G_{12} (MPa)
4504	1916	0.32	0.45	660.64

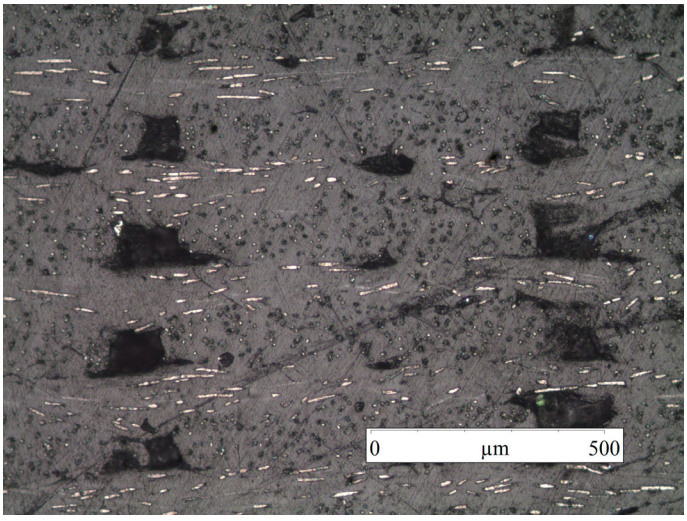

FIGURE 9 Printed coupon with 0/90 configuration and magnification 10×.

25778196, 0, Downloaded from https://onlinelibrary.wiley.com/doi/10.1002/eng2.12799 by Universidad De Sevilla, Wiley Online Library on [08/11/2023]. See the Terms and Conditions (https://onlinelibrary.wiley.com/terms-and-conditions) on Wiley Online Library for rules of use; OA articles are governed by the applicable Creative Commons License

4.2 | Numerical results

The coupled FEM model developed in the previous sections and the properties obtained in the reverse engineering procedure are used herein. The model provides the numerical stress versus strain curves analogous to those of the test campaign (in the initial elastic part). Figure 10 shows the a_{11} component of the orientation tensor (for both toolpath configurations) obtained after the mapping between meshes (manufacturing and structural model). It is interesting to notice that the model is also able to capture the orientation of the filaments in the wall zones (specimen perimeter). Table 3 summarizes the maximum, minimum and mean apparent stiffness associated with both toolpath configurations analyzed in the experimental test campaign and the one obtained from the numerical model.

As a result of the virtual testing, the experimental and numerical stress versus strain curves are compared in Figure 11. Discontinuous lines are associated to experimental results. It can be concluded that for both configurations an acceptable fit between numerical and experimental results is observed at the initial linear elastic zone. It should be noticed that from a design point of view an adequate characterization of the elastic properties is very important. Experimental results show a non-linear behavior for strain values larger than 0.5%. Thus, numerical results do not remain valid out this range. It is interesting to recall that estimated properties allow to capture that the 0/90 configuration model present a significantly higher stiffness than +45/−45 configuration model.

Moreover, in order to validate the initial hypothesis that for an adequate simulation of 3D printed parts, the printed filament should include a transversely isotropic behavior. Two additional numerical models are done assuming an isotropic filament behavior based on the manufacturer's own properties ($E = 2.4$ GPa, $\nu = 0.3$).[22] The other numerical parameters (toolpath, mesh) were the same. Figure 11 also shows the curves obtained for the 0/90 and +45/−45 configurations when isotropic behavior is assumed. It is interesting to notice that both curves including isotropic behavior are superimposed for both toolpath configurations. Thus, an anisotropic character should be taken into account for capturing the toolpath effect showed by experimental results.

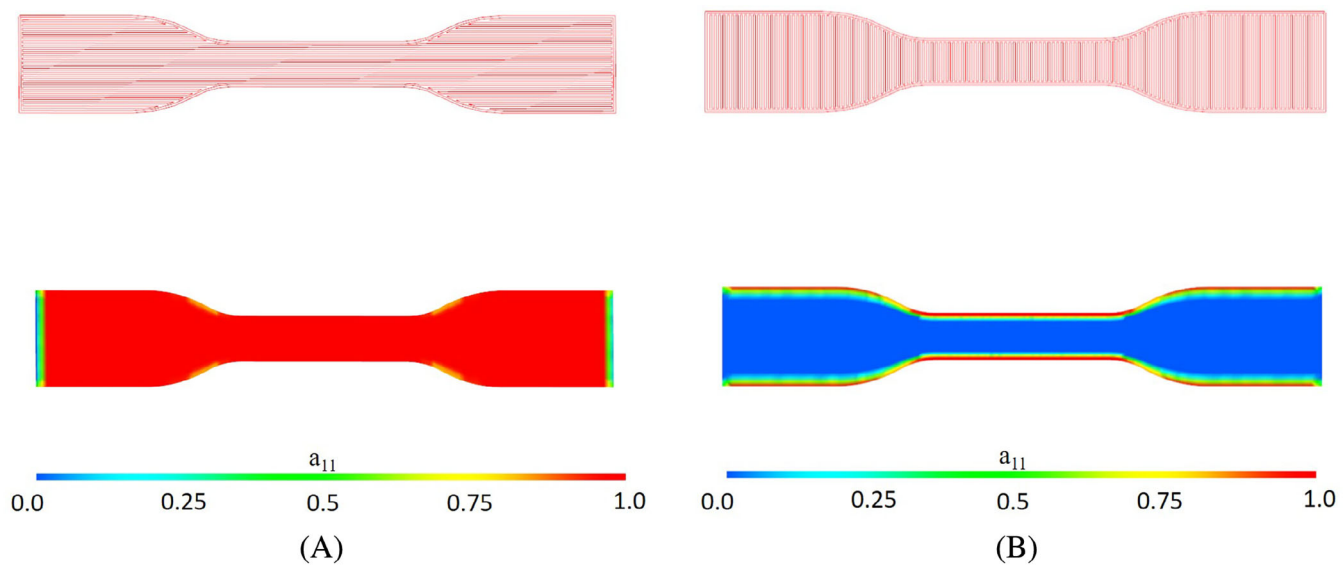

FIGURE 10 a_{11} component of the orientation tensor for an intermediate layer oriented (A) 0° and (B) 90°.

TABLE 3 Apparent stiffness obtained experimentally and numerically.

	Experimental			Numerical
Configuration	**Min**	**Max**	**Mean**	**RevEng**
0/90 (MPa)	3053	3671	3277	3277
+45/−45 (MPa)	2087	2639	2376	2377

25778196, 0, Downloaded from https://onlinelibrary.wiley.com/doi/10.1002/eng2.12799 by Universidad De Sevilla, Wiley Online Library on [08/11/2023]. See the Terms and Conditions (https://onlinelibrary.wiley.com/terms-and-conditions) on Wiley Online Library for rules of use; OA articles are governed by the applicable Creative Commons License

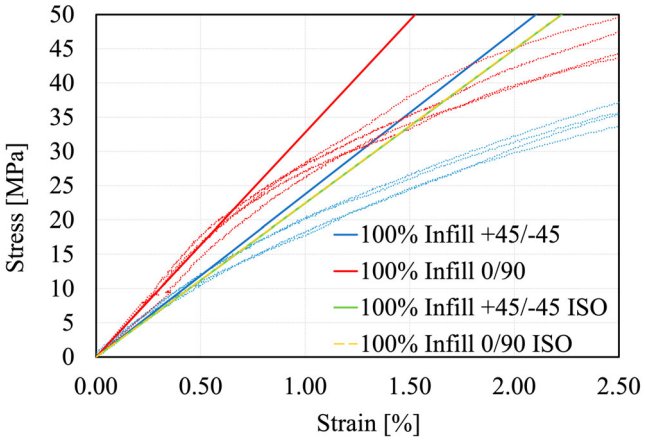

FIGURE 11 Numerical-experimental correlation. Coupled analysis using implicit FEA solver.

5 | MODELING POROSITY EFFECT ON 3D PRINTED PARTS

Using the proposed coupled numerical model, the effects of the porosity induced by the FDM process is analyzed from a numerical point of view. Specifically, the tool is applied to (a) elucidate the effects that the infill percentage and pattern have on the stiffness of the specimen and (b) analyze the presence of porosity due to filament deposition.

5.1 | Infill percentage and pattern

The effect on the global structural response of a specimen with an infill percentage lower than 100% and with triangular and hexagonal geometric patterns is analyzed. It should be noticed that from a simulation point of view this effects are included as a porosity phase. Thus, the trajectory patterns that generate the infill patterns under study are implemented on the same geometrical model by means of Eiger. The additive manufacturing scheme consists of 20 layers of 0.1 mm thickness. The printer impose that the bottom and top layers (two layers each) must be 100% infill and with a +45/−45 pattern for an adequate support of the inner lattice patterns. Then, the remaining layers (16) are printed following a triangular or hexagonal lattice pattern. Figure 12 shows the pictures of the design of the analyzed patterns for an intermediate layer.

Then, the mapping is carried out following the procedure described in the previous sections, transferring the toolpath data to the integration points of the mesh of the structural problem. The FEM model of this section also includes the orientation tensor and also defines a new phase which is the porosity associated with the infill percentage and pattern. Thus, a set of elements with null stiffness is generated. In Figure 13, the local porosity phase associated to one of the internal layers is presented.

The presence of the porosity phase results in a variation of the apparent stiffness of the specimens. Numerical results are shown in Figure 14. As expected, a decrease of the infill percentage derives in a decrease of the apparent stiffness. The differences reduces when lattice structures are used. In particular, the apparent stiffness for hexagonal pattern specimens with 37% and 50% infill percentage is very similar. Regarding the shape of lattice patterns, the triangular pattern shows an overall stiffer behavior (due to its geometrical shape). It is also interesting to verify that numerical results are different when anisotropy effects are taken into account. Thus, it can be concluded that we cannot exclude this effect when modeling 3D printed parts.

5.2 | Porosity effect due to filament deposition

At the meso-scale level, the model can take into account the effect of porosity associated with the RVE. Typically 3D printed parts present a lattice type microstructure, which is characterized at the RVE modeling level with the following parameters:

25778196, 0, Downloaded from https://onlinelibrary.wiley.com/doi/10.1002/eng2.12799 by Universidad De Sevilla, Wiley Online Library on [08/11/2023]. See the Terms and Conditions (https://onlinelibrary.wiley.com/terms-and-conditions) on Wiley Online Library for rules of use; OA articles are governed by the applicable Creative Commons License

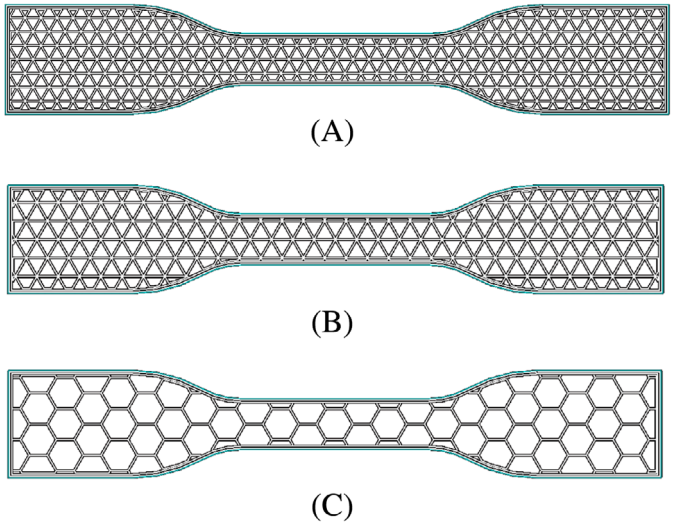

FIGURE 12 Analysed infill patterns designed in Eiger. (A) Triangular pattern 50% infill. (B) Triangular pattern 37%. (C) Hexagonal pattern 37%.

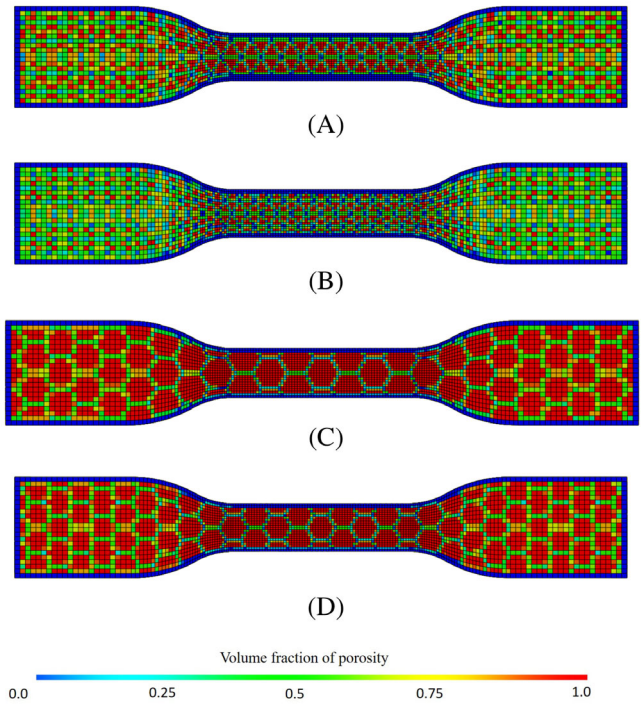

FIGURE 13 Porosity infill mapped. (A) Triangular pattern 37% infill. (B) Triangular pattern 50%. (C) Hexagonal pattern 37%. (D) Hexagonal pattern 50%. (E) Material density countour.

1. Filament width to filament height ratio.
2. Bonded line percentage of the deposited filament in the RVE height direction.
3. Bonded line percentage of the deposited filament in the RVE width direction.

In order to analyze this effect, a modified RVE has been generated on the 0/90 configuration, see Figure 15. Thus, an RVE with the same filament width to filament height ratio equals to 1:5 and relative bonded height equal to 0.2 have been set. It should be noticed that, changes in the bonded area percentage results in larger voids. Thus, two relative bonded

25778196, 0, Downloaded from https://onlinelibrary.wiley.com/doi/10.1002/eng2.12799 by Universidad De Sevilla, Wiley Online Library on [08/11/2023]. See the Terms and Conditions (https://onlinelibrary.wiley.com/terms-and-conditions) on Wiley Online Library for rules of use; OA articles are governed by the applicable Creative Commons License

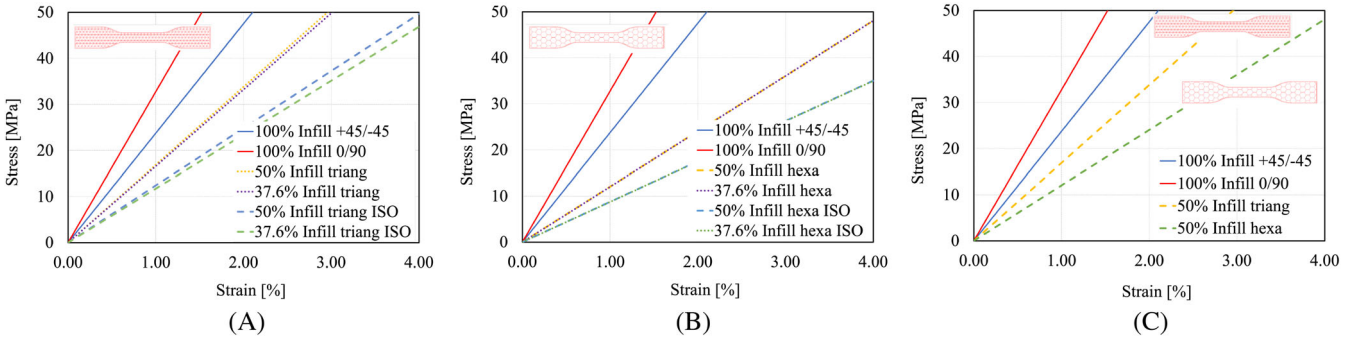

FIGURE 14 Infill pattern effect. (A) Triangular pattern. (B) Hexagonal pattern. (c) Comparative lattice shape.

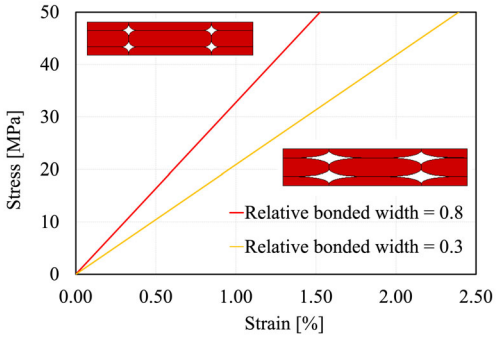

FIGURE 15 Porosity effect due to filament deposition.

width are compared: (a) the default value 0.8 and (b) 0.3 which represent large pores as those observed in the microscope. In view of the numerical results presented in Figure 15, it can be concluded that modifications in the height/width ratios and the bonded line percentage can significantly modify the apparent stiffness of the specimen.

6 | CONCLUSIONS

A numerical study has been presented with the aim of generating a simulation tool able to include the filament anisotropy and toolpath effects of 3D printed parts. In particular, transversely isotropic behavior for the short fibre reinforced plastic material (Onyx) used in FDM manufacturing is analyzed. This numerical approach is validated with experimental results. Then, a virtual test model is obtained that couples the manufacturing problem with the structural FEM model. This model can include the microstructure induced by the additive manufacturing process itself.

It is concluded that, even for Onyx parts with 100% infill, a different global structural response is observed depending on way the filaments are deposited. This anisotropic behavior, observed in Reference 23, is analyzed numerically in this paper for two different stacking sequences. Based on experimental results and using a reverse engineering procedure the linear elastic transversely isotropic parameters of each printed filament are obtained.

The effect of the porosity phases associated with the infill percentage and pattern are also analyzed. An adequate characterization of this variables will allow engineers to define customized designs in terms of stiffness criteria.

As future possibilities, the use of this numerical approach may help in precisely characterize the fracture properties of this kind of materials. This characterization is essential in applications where damage is expected and it also may allow to reinforce where needed. Thus, this numerical tool is a step towards an accurate and reliable characterization of the properties and designs, allowing to introduce 3D printed parts in primary structures with extended safety requirements. The actual limitations of the proposed model is that it only models the initial linear behavior. Nevertheless, from a design point of view, it is always desirable that parts work only on linear elastic regime.

25778196, 0, Downloaded from https://onlinelibrary.wiley.com/doi/10.1002/eng2.12799 by Universidad De Sevilla, Wiley Online Library on [08/11/2023]. See the Terms and Conditions (https://onlinelibrary.wiley.com/terms-and-conditions) on Wiley Online Library for rules of use; OA articles are governed by the applicable Creative Commons License

Future studies could analyze more complex geometries such as sandwich structures that includes top and bottom laminates and an intermediate zone with honeycomb patterns. Further numerical analysis may also focus in the nonlinear part of the stress-strain behavior of the printed filaments. The nonlinearity could be associated to the plasticisation and/or the damage of the matrix.

AUTHOR CONTRIBUTIONS

Alejandro Estefani: data curation (equal); formal analysis (equal); investigation (equal); methodology (equal); software (equal); supervision (equal); validation (equal); visualization (equal); writing – original draft (equal); writing – review and editing (equal). **Luis Távara:** conceptualization (lead); data curation (equal); formal analysis (equal); funding acquisition (lead); investigation (equal); methodology (equal); project administration (equal); resources (equal); software (equal); supervision (equal); validation (equal); visualization (equal); writing – original draft (equal); writing – review and editing (equal).

ACKNOWLEDGMENTS

This study was partially supported by the Spanish Ministry of Economy and Competitiveness and European Regional Development Fund (PID2021-123325OB-I00).

CONFLICT OF INTEREST STATEMENT

The authors declare no potential conflict of interest.

PEER REVIEW

The peer review history for this article is available at https://publons.com/publon/10.1002/eng2.12799.

DATA AVAILABILITY STATEMENT

Data is available on request.

ORCID

Luis Távara https://orcid.org/0000-0001-6825-4099

REFERENCES

1. Margolis JM. *Engineering Thermoplastics: Properties and Applications*. Marcel Dekker Inc.; 1985.
2. Tian X, Liu T, Wang Q, Dilmurat A, Li D, Ziegmann G. Recycling and remanufacturing of 3D printed continuous carbon fiber reinforced PLA composites.J clean. *Prod*. 2017;142:1609e18. doi:10.1016/j.jclepro.2016.11.139
3. Ahmad MN, Ishak MR, Taha MM, Mustapha F, Leman Z. Investigation of ABS–oil palm fiber (Elaeis guineensis) composites filament as feedstock for fused deposition modeling. *Rapid Prototyp J*. 2023;29(5):897-909.
4. Lau K-T, Taha MM, Rashid NHA, Manogaran D, Ahmad MN. Effect of HBN fillers on rheology property and surface microstructure of ABS extrudate. *J Teknol*. 2022;84(4):175-182.
5. Hague R, Campbell I, Dickens P. Implications on design of rapid manufacturing. *J Mech Eng Sci*. 2003;217(1):25-30.
6. Preuß H, Vietor T. Design for fiber-reinforced additive manufacturing. *J Mech des*. 2015;137(11):111409.
7. Murr LE. Frontiers of 3D printing/additive manufacturing: from human organs to aircraft fabrication. *J Mater Sci Technol*. 2016;32:987-995.
8. Munhoz R, Moraes CAC, Tanaka H, Kunkel ME. A digital approach for design and fabrication by rapid prototyping of orthosis for developmental dysplasia of the hip. Research on. *Biomed Eng*. 2016;32(1):63-73.
9. Herbert N, Simpson D, Spence WD, Ion W. A preliminary investigation into the development of 3-D printing of prosthetic sockets. *J Rehabil Res Dev*. 2005;42(2):141.
10. Ferroa C, Grassia R, Seclìb C, Maggiorea P. Additive manufacturing offers new opportunities in UAV research. Paper presented at: 48th CIRP Conference on Manufacturing Systems-CIRP CMS; 2016:2015:1004-1010.
11. Gokhale R, Wan Y, Mehndiratta M, Kayacan E. Fixed-wing vertical takeoff and landing UAV with additive manufacturing: a dual-rotor version. Proceedings of the 3rd International Conference on Progress in Additive Manufacturing; Pro-AM. 2018 250-255.
12. Melenka GW, Cheung BKO, Schofield JS, Dawson MR, Carey JP. Evaluation and prediction of the tensile properties of continuous. *Compos Struct*. 2016;153:866-875.
13. Ning F, Cong W, Hu Y, Wang H. Additive manufacturing of carbon fiber-reinforced plastic composites using fused deposition modeling: effects of process parameters on tensile properties. *J Compos Mater*. 2017;51(4):451-462.
14. Tian X, Liu T, Yang C, Wang Q, Li D. Interface and performance of 3D printed continuous carbon fiber reinforced PLA composites. *Compos Part A: Appl Sci Manuf*. 2016;88:198-205.

25778196, 0, Downloaded from https://onlinelibrary.wiley.com/doi/10.1002/eng2.12799 by Universidad De Sevilla, Wiley Online Library on [08/11/2023]. See the Terms and Conditions (https://onlinelibrary.wiley.com/terms-and-conditions) on Wiley Online Library for rules of use; OA articles are governed by the applicable Creative Commons License

15. Lopes CS, Gurdal Z, Camanho PP. Variable-stiffness composite panels: buckling and first-ply failure improvements over straight-fibre laminates. *Comput Struct*. 2008;86:897-907.
16. Iragi M, Pascual-Gonzalez C, Esnaola A, Lopes CS, Aretxabaleta L. Ply and interlaminar behaviours of 3D printed continuous carbon fibre-reinforced thermoplastic laminates; effects of processing conditions and microstructure. *Addit Manuf*. 2019;30:100884.
17. Plocher J, Wioland J, Panesar AS. Additive manufacturing with fibre reinforcement design guidelines and investigation into the influence of infill patterns. *Rapid Prototyp J*. 2022;28(7):1241-1259.
18. Ferreira RTL, Amatte IC, Dutra TA, Bürger D. Experimental characterization and micrography of 3D printed PLA and PLA reinforced with short carbon fibers. *Compos Part B: Eng*. 2017;124:88-100.
19. Junaedi H, Baig M, Dawood A, Albahkali E, Almajid A. Mechanical and physical properties of short carbon fiber and nanofiller-reinforced polypropylene hybrid nanocomposites. *Polymers*. 2020;12:2851. doi:10.3390/polym12122851
20. Isobe T, Tanaka T, Nomura T, Yuasa R. Comparison of strength of 3D printing objects using short fiber and continuous long fiber. *IOP Conf. Series Mater Sci Eng*. 2018;406:012042.
21. Yasa E, Ersoy K. Dimensional accuracy and mechanical properties of chopped carbon reinforced polymers produced by material extrusion additive manufacturing. *Mater (Basel)*. 2019;12(23):3885.
22. Markforged. https://markforged.com, 2022.
23. Tavara L, Madrigal C, Aranda MT, Justo J. Anisotropy and ageing effect on the mechanical behaviour of 3D-printed short carbon-fibre composite parts. *Compos Struct*. 2023;321:117196.
24. Górski F, Wichniarek R, Kuczko W, Zawadzki P, Buń P. Strength of abs parts produced by fused deposition modelling technology. A critical orientation problem. *Adv Sci Technol*. 2015;9(26):12-19.
25. Ahn SH, Montero M, Odell D, Round S, Wright PK. Anisotropic material properties of fused deposition modeling ABS. *Rapid Prototyp*. 2002;8(4):248-257.
26. Sangaletti S, García IG. Fracture tailoring in 3D printed continuous fibre composite materials using the phase field approach for fracture. *Compos Struct*. 2022;300:116127.
27. Ghandriza R, Hartb K, Lia J. Extended finite element method (XFEM) modeling of fracture in additively manufactured polymers. *Addit Manuf*. 2020;31:100945.
28. Lia RJ, Yanga S, Lib D, Chalivendraa V. Numerical and experimental studies of additively manufactured polymers for enhanced fracture properties. *Eng Fract Mech*. 2018;204:557-569.
29. Mirkhalaf SM, van Beurden TJH, Ekh M, Larsson F, Fagerström M. An FE-based orientation averaging model for elasto-plastic behavior of short fiber composites. *Int J Mech Sci*. 2022;219:107097.
30. Digimat. User's Manual. 2021.
31. ABAQUS. *ABAQUS User's Manual*. Dassault Systèmes. Simulia Corporation ABAQUS vs; 2019:19.
32. American Society for Testing and Materials. Standard test method for tensile properties of plastics. *ASTM D638-10*. 2010;D638e710. doi:10.1520/D0638-10
33. Saeed K, McIlhagger A, Harkin-Jones E, Kelly J, Archer E. Predication of the in-plane mechanical properties of continuous carbon fibre reinforced 3D printed polymer composites using classical laminated-plate theory. *Compos Struct*. 2021;259:113226.
34. Kriz RD, Stinchcomb WW. Elastic moduli of transversely isotropic graphite fibers and their composites. Department of Engineering Science and Mechanics, Virginia Polytechnic Institute and State University, Blacksburg, VA 24061. 1978.

How to cite this article: Estefani A, Távara L. Numerical multiscale analysis of 3D printed short fiber composites parts: Filament anisotropy and toolpath effects. *Engineering Reports*. 2023;e12799. doi: 10.1002/eng2.12799

25778196, 0, Downloaded from https://onlinelibrary.wiley.com/doi/10.1002/eng2.12799 by Universidad De Sevilla, Wiley Online Library on [08/11/2023]. See the Terms and Conditions (https://onlinelibrary.wiley.com/terms-and-conditions) on Wiley Online Library for rules of use; OA articles are governed by the applicable Creative Commons License